USE OF RARE-EARTH TRACERS AS PU SURROGATES IN ISV STUDIES*

August W. Cronenberg
Engineering Science & Analysis
Albuquerque, NM 87110

Richard McAtee and Richard Callow
Idaho National Engineering Laboratory
EG&G Idaho, Inc.
Idaho Falls, ID 83415

ABSTRACT

Two in situ vitrification (ISV) field tests were conducted at the Idaho National Engineering Laboratory (INEL) to assess ISV suitability for long-term stabilization of buried radioactive waste. Small amounts of rare-earth oxides (tracers: Dy_2O_3, Yb_2O_3, Tb_4O_7) were added to soils to simulate buried PuO_2. Test data indicate partial release of such tracers, which poses the question of whether similar release might occur for PuO_2. This paper presents an evaluation of the INEL release data and the applicability of using such tracers as surrogates for PuO_2.

A comparison of the chemical and thermodynamic properties of the rare-earth oxides, as well as predictions of binary diffusivities and Sherwood numbers, indicates similarity of molecular transport and chemical properties. Thus, the mechanism(s) responsible for rare-earth oxide release also applies to PuO_2. To quantify the INEL tracer release data, an assessment was made of three potential transport mechanisms: diffusion through a stagnant pool, mass transport by convective currents, and molecular release by escaping gas bubbles. Analysis indicates that tracer carry-off by escaping gas would be the dominant release mechanism for the INEL test conditions. These results compare favorably with the INEL data trends. In the first test, IFT-1, a maximum of ≈4% tracer release occurred during soil melting and associated off-gassing, while essentially nil release was observed for the second experiment (IFT-2) for which off-gassing was much reduced.

INTRODUCTION

A comprehensive in situ vitrification (ISV) testing and feasibility program is being conducted at the Idaho National Engineering Laboratory (INEL), as part of Department of Energy (DOE) efforts at improving long-term stabilization of buried radioactive waste. The process utilizes electrical resistance heating to melt either contaminated soil or buried waste in place, which upon resolidification fixes the waste into a glass-like form. Two Intermediate Field Tests (IFT) have been conducted at the INEL to date to assess overall ISV process performance. A detailed description of these two tests are presented elsewhere (1,2); here an assessment is made of the tracer release data and its applicability to plutonium release behavior.

In the INEL tests, small quantities of rare-earth oxides (tracer material: Dy_2O_3, Yb_2O_3, Tb_4O_7) were added to the test pits to simulate plutonium (Pu) behavior. The interest in plutonium stems from the necessity to protect ISV workers and equipment from its release during soil melting. Some data are available on Pu release from ISV melts; however, these data are limited to vitrification of contaminated soils (3). The interest in the INEL studies is the application of the ISV process to remediation of buried waste canisters which contain various metals, sludge, and combustible materials contaminated with trace quantities of plutonium. It is from this perspective that small quantities of rare-earth tracers were added to the INEL test pits.

In the first experiment, IFT-1, three rare-earth tracers (Dy_2O_3, Yb_2O_3, and Tb_4O_7) were added to the test pit, while in the second experiment (IFT-2) only Dy_2O_3 was used to simulate PuO_2 behavior. Data from IFT-1 indicate tracer release upwards of 4% during soil melting and associated off-gassing, while essentially nil release was observed for IFT-2 where off-gassing was much reduced. Thus, questions arise as to the conditions governing release and whether the tracers employed adequately simulate the chemical/transport properties of PuO_2 in ISV environments. In this paper we attempt to answer such questions.

In the next section, the IFT test conditions and release data are summarized, followed by a discussion of the high-temperature chemistry of the rare-earth oxides compared with that of PuO_2. Analysis of mass transport phenomena for ISV melt conditions are then presented, where theoretical predictions of rare-earth tracer release are compared with data trends. Conclusions are then summarized.

TEST DESCRIPTION

During the summer of 1990, two Intermediate Field Tests (IFT) were conducted (1,2) using rare-earth tracers to simulate transuranic behavior during soil melting. Figure 1 illustrates the relative positioning of waste and tracers used in the IFT-1 and IFT-2 experiments. Pertinent inventory information is provided in Table I, where it is noted that IFT-2 contained about twice the inventory of Dy_2O_3 (but no Tb_4O_7 or Yb_2O_3) and significantly more vaporous material

* Work supported by the U.S. Department of Energy, Office of Environmental Restoration and Waste Management, under DOE Idaho Field Office, Contract DE-AC07-76ID01570.

(combustible and water) than in IFT-1. Figure 2 illustrates the depth of melting as a function of time for each test, deduced from knowledge of the average electrode depth.

After testing, the amounts of tracers were measured in retrieved samples of vitrified soil, as well as at various locations within the collection hood, off-gas piping surfaces, scrub solution, and HEPA filters (collectively referred to as the off-gas collection system). Although quantitative determination of tracer amounts was hampered by sampling uncertainties, results indicate that the majority of the tracers were retained in the vitrified product. Nevertheless, several percent of the tracer material were found within the off-gas collection system for IFT-1 as shown in Table II.

Though the IFT-2 test contained about twice the inventory of Dy_2O_3 compared to IFT-1 (the total tracer inventory in IFT-1 was 4004 g versus 2282 g for IFT-2), essentially nil dysprosium was found in the IFT-2 off-gas collection system. Also note that although IFT-2 contained potentially more volatile waste then IFT-1, a comparison of hood temperature and vacuum pressure measurements indicate a reduced gas release process in IFT-2 than for IFT-1. As indicated in Fig. 3, the IFT-2 data show only three negative spikes in hood vacuum pressure and a corresponding temperature increase, versus 14 spiking events for IFT-1. These data suggest a more dynamic off-gassing process for the IFT-1 test, which may have been responsible for enhanced tracer release noted in that experiment.

TRACER SUITABILITY

As part of an assessment of chemical similarities between plutonium compounds and the rare earths (lanthanides), a review of published literature was performed. Basic chemical similarities have resulted in previous use of rare earths as Pu surrogates; however, the ISV environment is one of high temperature ($>1500°C$) where applicable data are scarce.

To determine the most likely chemical form of plutonium for ISV environments, a review of Pu oxidation states at high temperature was performed. Results indicate that at ISV temperatures and basalt melt compositions, a reducing environment (indicated by $Fe^{+2}/\Sigma Fe > 0.9$) exists; thus, the most likely forms of Pu would be PuO_2 (oxidation state +4) and Pu_2O_3. A review of the chemistry for the rare earths indicate similar oxidation states, i.e., +2 to +4.

With respect to solubility similarities, previous studies indicate that oxides of both Pu (4) and the rare earths (5,6) are soluble in iron-rich basalt to at least 1 wt%. This limit far

TABLE I

Waste inventory in the IFT-1 and IFT-2 Experiments

Material	Inventories	
	IFT-1	IFT-2
Waste Materials		
Combustible	302 kg	688 kg
Water	217 kg	469 kg
FLOOR-DRI	20 kg	43 kg
MICRO-CELL	65 kg	140 kg
Metal	1,122 kg	3,065 kg
Glass	220 kg	108 kg
Concrete	393 kg	272 kg
Tracers		
Dy_2O_3	1.336 kg	2.282 kg
Tb_4O7	1.337 kg	---
$Yb2O_3$	1.331 kg	---
Tracers (total)	4.004 kg	2.282 kg
Soil		
Soil Fill	24,780 kg	22,662 kg
Soil Overburden	0.6 m (2 ft)	1.2 m (4 ft)

TABLE II

IFT-1 Tracer Release Data

Oxide Inventory	Rare Earth	Hood/Duct Deposits	Scrub Deposits	Max. Release Fraction
Dy_2O_3 = 1336 g	Dy = 1164 g	4.7-6.2 g	7.5 g	0.012
Tb_4O_7 = 1337 g	Tb = 1137 g	28-29.9 g	14.0 g	0.039
Yb_2O_3 = 1331 g	Yb = 1169 g	11-12.3 g	17.5 g	0.025
Total = 4004	Total = 3473 g			Avg. = 0.025

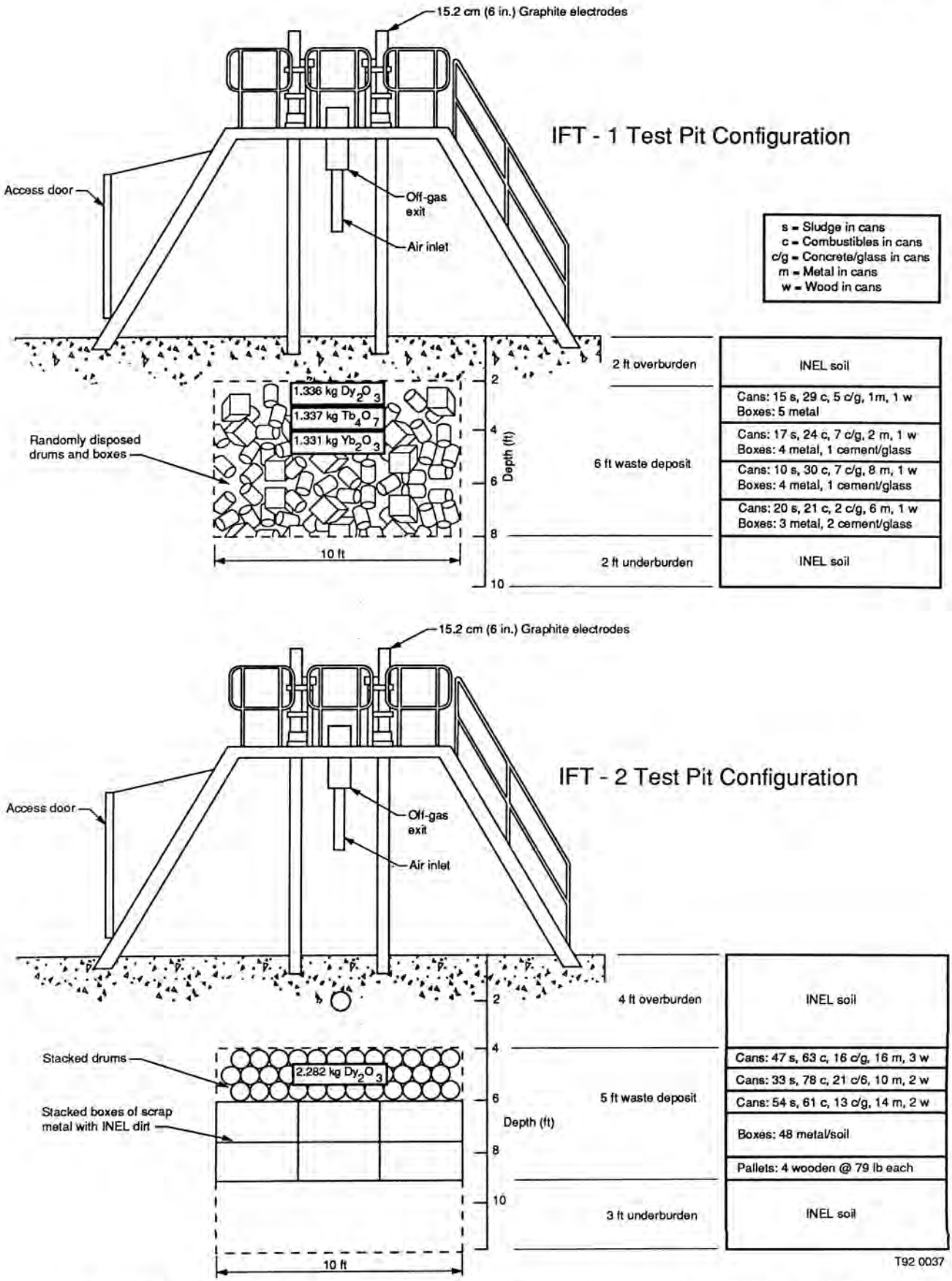

Fig. 1. Illustration of waste configuration and tracer placement location in Tests IFT-1 and IFT-2.

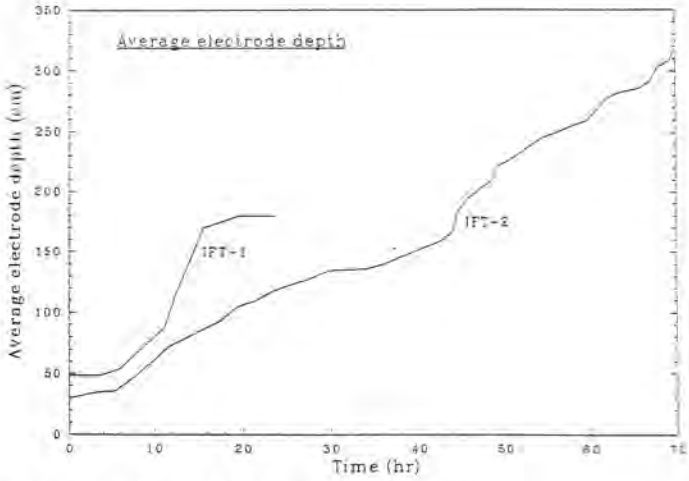

Fig. 2. Depth of soil melting, deduced from average electrode depth data.

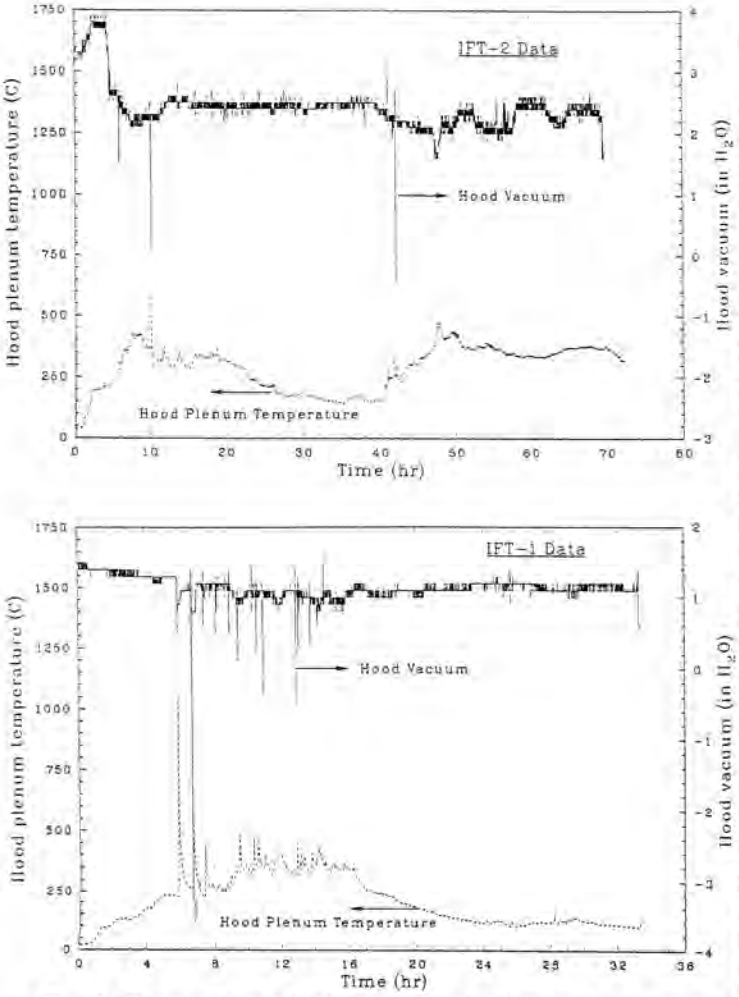

Fig. 3. Comparison of off-gassing behavior noted in tests IFT-1 and IFT-2.

exceeds what would be expected for ISV conditions, so that similar solubility characteristics are indicated for PuO_2 and the rare-earth tracers (Dy_2O_3, Yb_2O_3, Tb_4O_7). Thus, the rare-earth oxides appear to be suitable surrogates for plutonium under ISV melt conditions.

SCOPING ANALYSIS

An assessment of the tracer release data can be approached from consideration of the fundamental equation for mass transport from a liquid pool, which is expressed by the following equation:

$$m_{rel} = k_m A(C_{bulk} - C_{surface}) \quad \text{(Eq. 1)}$$

where m_{rel} is the rate of mass released from free surface (g/s), k_m is the overall mass transport coefficient (cm/s), A is the surface area for release (cm^2), C_{bulk} is the bulk concentration of species in the melt (g/cm^3), and $C_{surface}$ is the concentration at the melt surface (g/cm^3). The difficulty in application of the Eq. (1) lies in specification of k_m, which is largely dictated by governing physical conditions. For ISV conditions the three mechanisms illustrated in Fig. 4 were investigated, i.e., **diffusion** from a stagnant pool, mass transfer due to **convective currents**, and mass transport due to **bubble escape**.

Scoping calculations are first presented to identify which mechanism is predominant for ISV melt environments, followed by quantitative assessment of the mass transport conditions associated with the IFT-1 experiment.

Diffusion from a Stagnant Pool

For quiescent liquids, molecular diffusion by random motion occurs due to concentration gradients, where the ISV melt can be modeled as a hemispherical pool such that the mass transport coefficient (k_m) and associated release time constant (t_{diff}) can be approximated by the expressions:

$$k_m = \pi D/R_p \quad \text{(Eq. 2)}$$

$$t_{diff} = R_p/k_m \quad \text{(Eq. 3)}$$

where D is the diffusion coefficient (cm^2/s) and R_p is the pool radius (cm).

Convection Controlled Mass Transport

Thermal gradients arise during ISV melting, where the hottest region exists at the electrode and the coldest at the melt boundaries resulting in free convective currents within the melt. Exact solutions to such coupled heat/mass transfer conditions are available only for idealized geometries and restrictions on density driven flow patterns. Thus, common practice is to make use of similarity analysis in conjunction with experimental data, to estimate the overall mass transfer coefficient (k_m). For free convection, the following expressions are suggested for k_m and the associated time constant (7):

$$k_m = 0.36(D/R_p)(Ra\ Sc/Pr)^{0.23} \quad \text{(Eq. 4)}$$

$$t_{conv} = R_p/k_m) \quad \text{(Eq. 5)}$$

where Ra is the Rayleigh number ($g\beta QR_p^5/\alpha k\mu_k$), Sc is the Schmidt number (μ_k/D), Pr is the Prandtl number (μ_k/α), R_p is the pool depth (cm), g is the gravity constant (cm/s^2), β is the thermal expansion coefficient (K^{-1}), Q is the volumetric heat source (W/cm^3), α is the thermal diffusivity (cm^2/s), μ_k is the kinematic viscosity (cm^2/s), k is the thermal conductivity (W/cm-K), and D is the diffusion coefficient (cm^2/s).

Mass Transfer Due to Bubble Rise

Figure 4 illustrates the basic characteristics of tracer release due to gas generation and bubble rise. For ISV melts which contain sufficient quantities of vaporous material, spherical bubbles will form and rise through the melt

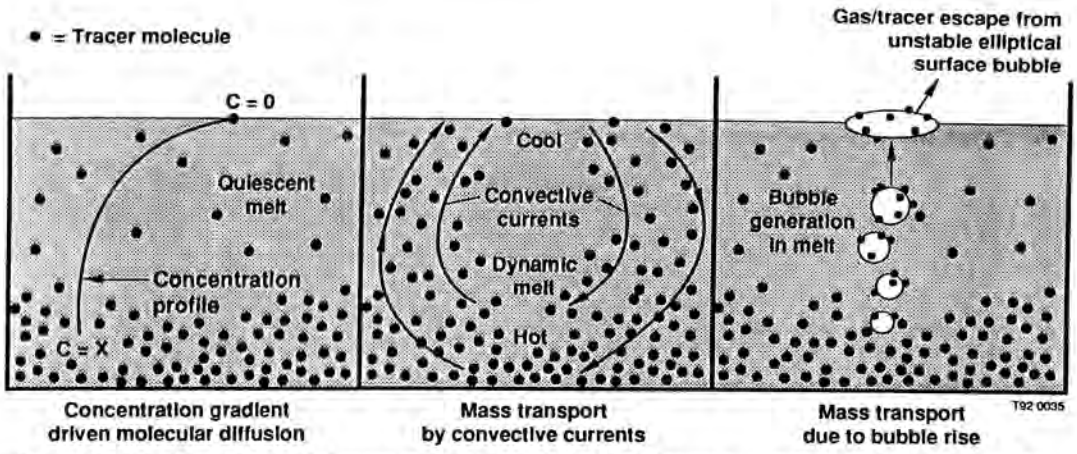

Fig. 4. Illustration of potential mass transport modes for quiescent, dynamic, and gaseous melts.

capturing tracer molecules in the process. Agglomeration of numerous bubbles at the melt surface leads to the formation of elliptical vapor domes, which become unstable with increased pressure releasing entrapped gas and tracers in the process. The limiting condition for such gas release is associated with the rate bubbles rise through the melt, where the terminal bubble velocity (V_t) and associated release time (t_{br}) express the condition where the forces of gravity and drag just balance that due to buoyancy:

$$V_t = 2R_b^2 \varrho_L g/9\mu \qquad \text{(Eq. 6)}$$

$$t_{br} = R_p/V_t \qquad \text{(Eq. 7)}$$

where R_p is the pool depth, R_b is the bubble radius, ϱ_L is the melt density, and the other parameters are as previously defined.

Scoping Predictions

Characteristic release times are given in Table III for prototypic ISV melt properties and system conditions. Although the results are simple order-of-magnitude estimates, diffusion times are clearly slow due to low diffusivities [0.5 x 10^{-6} cm^2/s, (8)] for basalt melts. The release time associated with convective currents within the internally heated pool (≈300 kW) is estimated to be much shorter than for diffusion; nevertheless, they are significantly longer than typical ISV melting times (one to two days). By contrast, the time associated with gas bubble rise is quite rapid, on the order of minutes. The indication of these results is that tracer release by carry-off with escaping gas bubbles (due to off-gassing of CO, CO_2, or water vapor) would be the dominant release mechanism for ISV melt conditions. Thus, a more detailed investigation of this process was investigated for the IFT-1 test conditions.

RELEASE PREDICTIONS FOR IFT-1 TEST CONDITIONS

Figure 5 presents evidence, taken from a video at the ISV melt surface, of gas escape from the ISV melt due to bursting of surface vapor domes. As illustrated in Fig. 4, formation of such an elliptical vapor dome can be visualized as the result of the agglomeration of numerous gas bubbles rising through the melt, which serve as carriers for tracer transport. Overpressurization and cyclic bursting of such surface bubbles thus leads to gas and tracer release. Quantitative assessment of the IFT-1 tracer release data can therefore be approached by estimating a characteristic bubble size for rise through the melt, and making use of empirically based mass-transport correlations for such bubble rise.

Minimum Bubble Size

Gas release from the melt is considered controlled by competition between buoyancy-driven bubble rise versus convective currents that tend to entrain the bubble within the melt pool. The terminal bubble velocity ($V_{t,rise}$) is given by Eq. (6), while the convective velocity (V_{conv})can be obtained from an energy balance and is given by:

$$V_{conv} = \left[\frac{2Q}{\rho_L A C_p \Delta T}\right] \qquad \text{(Eq. 8)}$$

where Q is the heating rate of pool (cal/s), ρ_L is the melt density (gm/cm^3), A is the pool cross-sectional area (cm^2), C_p is the melt heat capacity (cal/g-K), and ΔT is the temperature gradient from pool center to surface (K). By equating Eqs. (6) and (8), the **minimum bubble radius** ($R_{b,min}$) for escape is obtained:

$$R_{b,min} = \left[\frac{9Q\mu}{\rho_L^2 A C_p g \Delta T}\right]^{1/2}. \qquad \text{(Eq. 9)}$$

Calculational results for Eq. (9) are presented in Table IV at typical ISV heating rates of 300 kW and melt properties for INEL soil. As indicated for temperature differentials (ΔT) in the range of 50-300 K and viscosities (μ) of 300 poise, minimum bubble radii of ≈0.18 to 0.08 cm are predicted.

Maximum Bubble Size

Regardless of initial size, a bubble will grow due to a decrease in hydrostatic head as it rises through the melt, until it becomes large enough so that surface instabilities cause the bubble interface to become unstable. A frequently cited criterion for bubble breakup is that deduced by Levich (9), yielding the following expression for the maximum bubble size:

$$R_{b,max} = \frac{0.9\,(\sigma)}{V_T^2\,(\rho_g \rho_L^2)^{1/3}} \qquad \text{(Eq. 10)}$$

TABLE III

Summary of soil melt properties and system parameters

Properties of Molten Soil	Value
Soil Composition (wt%)	62-SiO_2/12-Al_2O_3/5-Fe_2O_3/20-other
Melt temperature (T_{mp})	1447°C (1720 K)
Density (ρ)	2.2 g/cm^3
Viscosity (μ)	300 poise
Kinematic viscosity ($\mu_k = \mu/\rho$)	136 cm^2/s
Thermal conductivity (k)	0.0335 cal/s-cm-K
Specific heat (C_p)	0.26 cal/g-K
Thermal diffusivity ($\alpha = k/\rho C_p$)	0.0585 cm^2/s
Thermal expansion coefficient (β)	3.1E-5 cm/cm-K (assumed)
Surface tension (σ)	1000 dy/cm (assumed)
Species diffusivity (D)	0.5x10^{-6} cm^2/s (assumed)
Assumed System Parameters	
R = ISV pool radius	= 100 cm (assumed)
V_p = pool volume	= 2.1E+6 cm^3
Q_e = power	= 300 kW (71,700 cal/s)
Q = volumetric heating rate	= 0.034 cal/cm^3-s
Release Mechanism	Characteristic Release Time
Diffusion	≈50,000 days
Free Convection	≈500 days
Bubble Escape	≈60 seconds

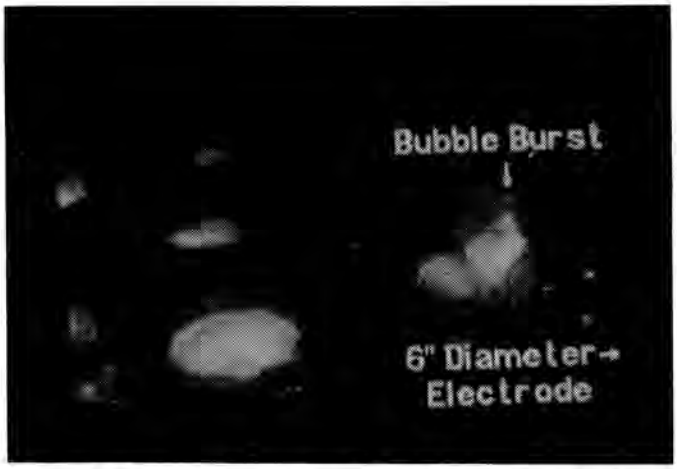

Fig. 5. Photographic evidence of bubble bursting at ISV melt surface.

where V_T is the terminal bubble velocity, σ is the surface tension dy/cm, and ρ_g and ρ_L are the densities of the vapor and liquid (gm/cm^3). Substitution of Eq. (6) into Eq. (10) yields the following expression for the maximum bubble radius:

$$R^5_{b,\max} = \frac{(18.2)\,(\sigma\mu^2)}{g^2\rho_L^2\,(\rho_g\rho_L)^{1/3}} \quad \text{(Eq. 11)}$$

Eq. (11) yields bubble radii of ≈5 cm. For present purposes only, bubbles sufficiently far removed from the effects of hydrodynamic instabilities are considered stable carriers for tracer release, i.e., $R_{b,max} \approx 2$ cm.

Mass Transport Coefficient for Bubble Rise

The overall mass transport coefficient (k_m) can be obtained from empirically based models for the Sherwood number (Sh) associated with spherical bubble rise through liquids, i.e.:

$$k_m = Sh(D)/d_b \quad \text{(Eq. 12)}$$

where d_b is the characteristic bubble diameter and Sh is found from the following correlations suggested in the literature (10):

$$Sh = 1.13\,(Pe^{1/2})\left[\frac{d_b}{0.45+0.2d_b}\right] \quad \text{(Eq. 13)}$$

$$Sh = 0.65\,Pe^{1/2} \quad \text{for Re} < 10 \quad \text{(Eq. 14)}$$

$$Sh = 1.13\left[1-\frac{2.96}{Re^{1/2}}\right]^{1/2} Pe^{1/2} \quad 100 \le Re \le 400 \quad \text{(Eq. 15)}$$

where Re is the bubble Reynolds Number ($V_b\rho_L d_b/\mu$), Pe is the bubble Peclet Number ($V_b d_b/D$), and Sh is the Sherwood Number ($k_m d_b/D$). The overall mass transfer rate due to bubble rise is obtained from Eq. (1), knowing the mass transport coefficient (k_m).

Table V summarizes "best estimate" calculations for the IFT-1 test conditions, using melt properties given in Table III and diffusivities of 0.1 - 0.5 x 10^{-6} cm^2/s. Release fractions of 4.5% to 20% are indicated, where the lowest value (4.5%) compares favorably with an experimental release of 3.9%. The 4.5% prediction is associated with the lower limit of bubble

TABLE IV

Estimation of Minimum Bubble Size for Escape From ISV Melts

Governing Equation:	
$R_{b,min} = [9Q\mu/\rho^2 AC_p g\Delta T]^{1/2}$	
Parameter Values:	
ρ = melt density	= 2.2 g/cm^3
Q = pool heating rate	= 300 KW = 7.17 E+4 cal/s
C_p = specific heat	= 0.26 cal/g-K
A = cross-sectional area	= 10 ft x 10 ft - 9.3 E+4 cm^2
g = gravity constant	= 980 cm/s^2
ΔT = temperature difference	= 50, 300 K
μ = viscosity	= 300 g/cm-s (poise)
Calculation:	
ΔT, K — $R_{b,min}$, cm	
50 — 0.184	
300 — 0.075	

size (d_b = 1 cm) and diffusivities of 0.10 x 10^{-6} cm^2/s. Since these values appear physically realistic, reasonable comparison between theory and the IFT-1 data are apparent, though from an order-of-magnitude perspective.

The principal parameter influencing calculational uncertainties is the absence of tracer and PuO_2 diffusivity (D) data for SiO_2-based melts. Until such data become available, exact predictions on tracer and Pu release cannot be made. Nevertheless, it is encouraging that use of published values (8) for the diffusivities of Ca and Si ions in SiO_2-based soils (D = 0.1-0.6 x 10^{-6} cm^2/s), yield tracer release fractions that are within measurement uncertainties associated with the ISV-IFT-1 tracer release data. Predictions (11) of the diffusivity of the tracers Dy_2O, Tb_4O_7, Yb_2O_3, and PuO_2 in SiO_2 melts yield similar values, that is approximately 0.3x10^{-6} to 0.6x10^{6} cm^2/s. Since the thermochemical and transport properties of PuO_2 are assessed to be similar to that of the rare-earth oxide tracers used in the IFT experiments, similar release of PuO_2 is predicted for dynamic off-gassing conditions, as occurred for the tracers.

Although IFT-2 contained potentially more volatile waste than IFT-1, the actual extent of gas release in IFT-2 was less than in IFT-1, based on hood temperature and vacuum pressure measurements. These data suggest that the tracer release is tied to the off-gassing phenomena, as supported by mass transport analysis.

One other noteworthy comment relates to differences in gas release mode, that is, gas release in the form of spherical bubbles (see Fig. 4) versus slug type gas release illustrated in Fig. 6. In the analysis presented here, well-defined bubble geometry was assumed, for which well-established empirical correlations are available for the Sherwood number (Sh) and associated mass transfer coefficient (k_m). For transient slug-type gas release, standard Sherwood number correlations would not apply; but rather the amount of released tracer material may best correlate to the quantity of ejected melt, which is difficult to predict "a priori." Nevertheless, the fact remains that the IFT-1 and IFT-2 tracer release data are best correlated to some form of gas release, whether it is transient off-gassing or quasi-steady bubble escape.

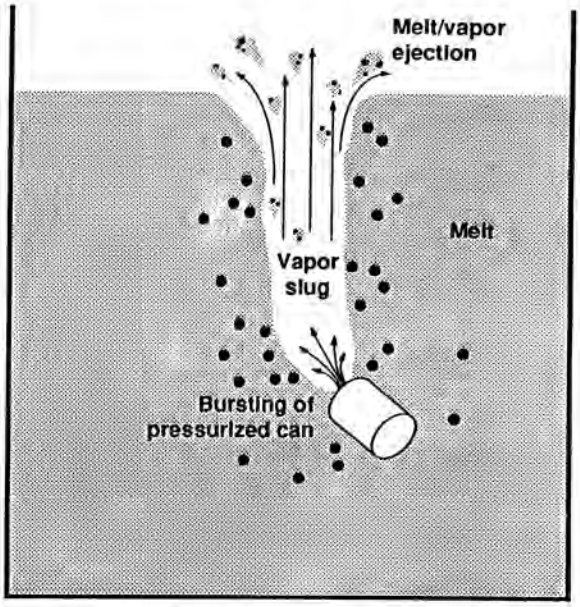

Fig. 6. Illustration of gas escape/melt ejection due slug-type gas release.

CONCLUSIONS

An assessment of the INEL IFT-1 and IFT-2 tracer release data leads to the following conclusions:

- The INEL tracer release for rare-earth oxides can be correlated to off-gassing behavior during ISV melting. The higher the degree of off-gassing the greater the potential for release of heavy oxides.
- Release of PuO_2 can be expected for similar off-gassing conditions, since its thermochemical and transport properties are similar to that of the rare-earth tracers used in the INEL studies.
- Uncertainties in predicted rare-earth oxides and PuO_2 release largely relate to lack of diffusivity (D) data for such species in basaltic melts.
- Relative heating rates and positioning of vaporous and tracer material, may account for differences in tracer release behavior noted in the IFT-1 and IFT-2 experiments. Slower heating rates and a greater depth of soil overburden appear to diminish oxide tracer release, while vaporization of volatiles buried below tracer material appears to enhance tracer release.
- Further analysis is suggested on the effects of transient-gas escape and associated melt ejection on tracer release behavior.

TABLE V

Mass Transport Predictions for IFT-1 Test Conditions

IFT-1 Test Conditions	Value
Melt surface area (A)	$\approx$ (10-ft x 10-ft) = 9.29E+4 cm^2
Bulk Concentration (C_{bulk})	= (3473 g)/(1.67E+7 cm^3) = 2.08 E-4 g/cm^3
Melt Time (t_{melt})	= 17.5 hr = 6.300 E+4 s

Bubble Velocity, Reynolds & Peclet Numbers

$V_b = 2R_b^2 \varrho_L g/9\mu$ $\quad Re = V_b(\rho)d_b/\mu$ $\quad Pe = = V_b d_b/D$

d_b, cm	V_b, cm/s	Re	Pe(D=0.5E-6 cm^2/s)	Pe(D=0.1E-6 cm^2/s)
1.0	0.40	0.003	8.0 E+5	4.00 E+6
4.0	6.39	0.187	5.1 E+7	2.56 E+8

Sherwood Number/Mass Transfer Coefficient/Release Rate

$Sh = 0.65Pe^{1/2}$ $\quad k_m$ (cm/s)= $Sh(D)/d_b$ $\quad m_{rel}(g/s)=k_m A(C_{bulk})$

	D = 0.5 E-6 cm^2/s			D = 0.1 E-6 cm^2/s		
d_b, cm	Sh	k_m	m_{rel}	Sh	k_m, cm/s	m_{rel}
1.0	581	2.90 E-4	0.0056	1300	1.30 E-4	0.0025
4.0	4647	5.81 E-4	0.0112	10400	2.60 E-4	0.0050

Total Mass/Fractional Release Estimates

$M_{rel}(g)=m_{rel}(t_{melt})$ $\quad RF=M_{rel}/(3473\ g)$

	D = 0.50 E-6 cm^2/s		D = 0.10 E-6 cm^2/s	
d_b, cm	M_{rel}, g	RF	M_{rel}, g	RF
1.0	353	0.10	158	0.045
4.0	707	0.20	315	0.091

REFERENCES

1. R. A. CALLOW and L. E. THOMPSON, "In Situ Vitrification: Application to Buried Waste," Proc. Waste Management Symp. 1991, Tucson, Az. (1991).
2. R. A. CALLOW et al., "In Situ Vitrification Application to Buried Waste: Final Report of Intermediate Field Tests at Idaho National Engineering Laboratory," EGG-WTD-9807, (1991).
3. J. L. BUELT et al., "In Situ Vitrification of Transuranic Wastes: Systems Evaluation and Applications Assessment," PNL-4800, (1987).
4. J. E. FLINN et al., "Annual Report on TRU Waste Form Studies with Special Reference to Iron-Enriched Basalt," EGG-FM-5366, (1981).
5. B. HESHMATPOUR, G. L. COPELAND, and R. L. HEESTAND, "Decontamination of Transuranic Waste by Melt Refining," ORNL/TM-7951, (1981).
6. C. W. HOBBICK, D. R. SCHALTZ, and G. D. ADEN, "Distribution and Removal of Radionuclides in Molten Stainless Steel," RHO-CD-1444, (1981).
7. D. A. PETTI et al., "Analysis of Fission Product Release Behavior from the TMI-2 Core," J. Nucl. Technology (87), pp. 243-263, (1989).
8. G. H. GEIGER and D. R. POIRIER, Transport Phenomena in Metallurgy, Addison-Wesley Pub. Co., Reading, MA (1973).
9. V. G. LEVICH, Physicochemical Hydrodynamics, Prentice Hall, pp. 452-454 (1962).
10. D. A. POWERS, J. E. BROCKMANN, and A. W. SHIVER, "VANESA: A Mechanistic Model for Radionuclide Release and Aerosol Generation During Core Debris Interactions with Concrete," NUREG/CR-4308, SAND85-1370, (1986).
11. A. W. CRONENBERG, "Predictions of Simulate and PuO_2 Release from ISV Melts," ESA-ISV-102-91, (1991).